New Insights of Polarization Beam Splitter Based on Sinusoidally Driven Directional Coupler

Akito Iguchi, *Member, IEEE*, and Yasuhide Tsuji, *Senior Member, IEEE*

***Abstract*—This paper studies on polarization beam splitter (PBS) in high-index-contrast waveguides based on sinusoidally driven directional coupler (SDDC), and offers new insights to realize compact and low-loss PBS with high fabrication tolerance. The PBS based on SDDC has advantage that power shift to an adjacent waveguide can be suppressed or totally banned by satisfying coherent destruction of tunneling (CDT) condition. However, in practical implementation, the PBS based on SDDC has trade-off relation between cross-talk of TE-like wave and loss of TM-like one. This paper investigates characteristics of the SDDC numerically, and shows possibility that cross-talk and loss can be suppressed, and small footprint can be achieved by position shift of DC-gap maintaining high fabrication tolerance.**

***Index Terms*—Polarization beam splitter (PBS), high-index-contrast waveguides, integrated optics.**

I. Introduction

TO REALIZE miniaturizing footprint of optical waveguide circuits, optical components in high-index-contrast (HIC) platform such as silicon on insulator (SOI) have been extensively studied. In the HIC platform, a polarization beam splitter (PBS) to control polarization is one of key devices for polarization diversity, and digital coherent transmission systems.

Many PBS concepts have been reported based on Mach-Zehnder interference (MZI) [1]–[3], multi mode interference (MMI) [4]–[6], and directional coupler (DC) [7]–[15]. Since MZI-based PBS consists of two power divider/combiner and phase shifting section, large footprint is required in longitudinal direction. MMI-based PBS also need large device size to synchronize light focus positions which are sensitive to wavelength, in addition, suppression of insertion loss is issue to be solved. DC-based PBS can be small footprint when waveguides have large polarization birefringence, but strong wavelength dependence and necessity of precise fabrication are widely pointed out.

In [15], PBS based on sinusoidally driven DC (SDDC) is numerically and experimentally demonstrated, and it is shown that SDDC can suppress crosstalk transmission in broadband wavelength region. Ideally, the SDDC can totally ban unwanted power coupling to an adjacent waveguide using phenomenon of coherent destruction of tunneling (CDT) [16]. Although in the HIC platform the coupling length of TE-like wave can be much longer than that of TM-like one ($L_{\mathrm{c,TM}} < L_{\mathrm{c,TE}}$), coupling of TE-like wave cannot be avoided, which results in suffering crosstalk. When TE-like wave satisfies CDT condition, coupling of TE-like wave can be prohibited and goes through port although TM-like one is coupled to cross port. However, in order to induce CDT, sinusoidal period Λ has to be small enough with respect to $L_{\mathrm{c,TE}}$, i.e, $\Lambda \ll L_{\mathrm{c,TE}}$. In [15], due to long sinusoidal period, crosstalk transmission of TE-like wave is not suppressed enough, thus there may be room of improvement.

In this paper, we investigate characteristics of the SDDC based PBS so as to achieve low-crosstalk, and small-footprint, and study on how to determine sinusoidal period.

In addition, we reveal that device length can be shortened and insertion loss can be suppressed by shifting position of DC gap. First, we numerically investigate Floquet-modes which are excited as super-modes in periodic SDDC. Based on relation between Λ and propagation loss of TM-like modes, we discuss how to determine optimal Λ. Next, we investigate characteristics of DC-gap-shifted SDDC, and show that the gap-shifting contributes to improving device performance.

II. Analysis of Sinusoidally Driven Directional Coupler (SDDC)

A. Analysis Model

The DC section of PBS investigated in this paper is shown in Fig. 1. Two parallel waveguides are adjacent to each other, and the center position $f(z)$ is sinusoidally deviated. $f_{\mathrm{g}}(z)$ indicates the center position of the gap in the SDDC, and r is a shifting coefficient. We consider the PBS where TE-like wave goes though the SDDC, and TM-like one is totally coupling to the adjacent waveguide. The gap and the oblong core width are let to be $g = 200$ nm and $w = 500$ nm, respectively. Core and cladding materials are assumed to be Si and SiO_2.

We numerically investigate two super modes that we call even-like and odd-like modes exited in the SDDC using a two dimensional finite element method (2DFEM) [17]. These super modes are just called even and odd modes in a straight DC waveguide, and the coupling length can be estimated by phase constants of these super-states. Core thickness, h, is taken into account using the effective index method (EIM) [18], and it is taken to be $h = 220$ nm. Refractive indices of SiO_2 ($n_{\mathrm{SiO_2}}$) and Si (n_{Si}) are determined by dispersion equations shown in [19] and [20], respectively. At wavelength of $\lambda = 1.55$ μm,

Manuscript received April 15, 2022; revised May 14, 2022; accepted May 23, 2022. Date of publication May 25, 2022; date of current version June 14, 2022. This work was supported by the Japan Society for the Promotion of Science KAKENHI under Grant JP 20K22408. *(Corresponding author: Akito Iguchi.)*

The authors are with the Department of Engineering, Muroran Institute of Technology, Hokkaido, Japan (e-mail: iguchia@mmm.muroran-it.ac.jp; y-tsuji@mmm.muroran-it.ac.jp).

Digital Object Identifier 10.1109/JPHOT.2022.3177787

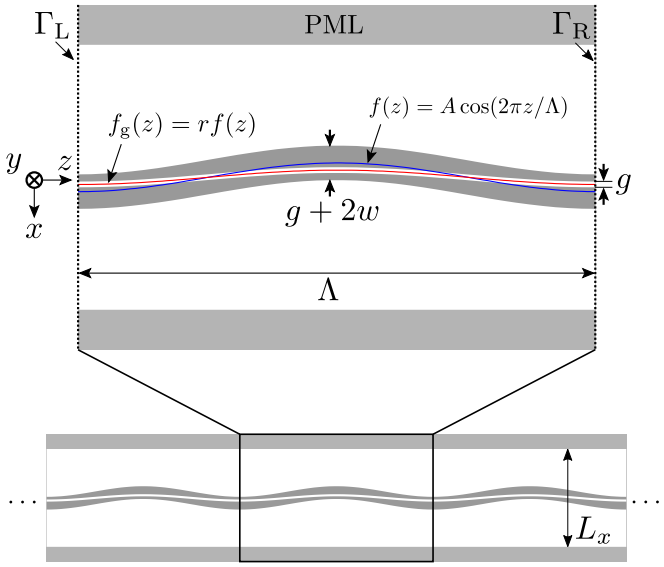

Fig. 1. A schematic of a periodic sinusoidally driven directional coupler (SDDC), and the definition of shifting coefficient r.

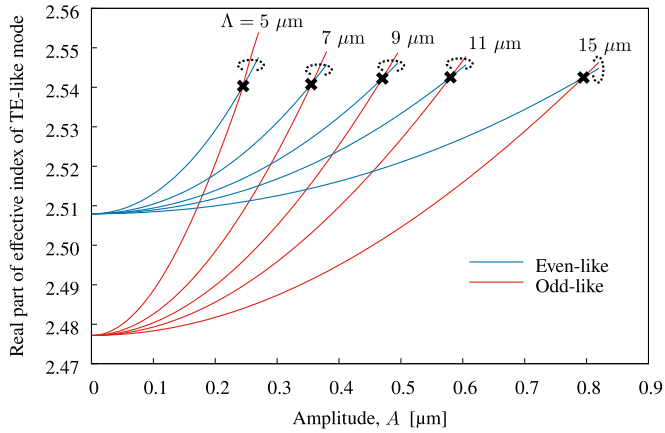

Fig. 2. Real part of effective index of TE-like super modes as a function of sinusoidal amplitude in the standard SDDC ($r = 1$) at $\lambda = 1.55$ μm.

$n_{SiO_2} = 1.444$, and the equivalent index of n_{Si} is 2.847 for TE-like wave, 2.053 for TM-like one. The physical window in x direction L_x is let to be 8 μm.

In the 2DFEM modal analysis, we solve the following quadratic eigenvalue equation obtained by imposing periodic condition at boundaries Γ_L and Γ_R, and factorizing a vector of electro-magnetic field $\{\phi\}$ into $\{\psi\}\exp(-j\beta z)$.

$$\left([K] + \beta\,[D] - \beta^2\,[M]\right)\{\psi\} = \{0\} \tag{1}$$

where $[K]$, $[D]$, and $[M]$ are system matrices, and β is a propagating constant. The detail of (1) is described in appendix. To obtain β of two super modes exited in the SDDC, we solve linearization form of (1).

$$([C] - \beta\,[G])\{\psi\}' = \{0\} \tag{2}$$

with

$$[C] = \begin{bmatrix} [D] & [K] \\ -[I] & [0] \end{bmatrix} \tag{3}$$

$$[G] = \begin{bmatrix} [M] & [0] \\ [0] & -[I] \end{bmatrix} \tag{4}$$

$$\{\psi\}' = \begin{bmatrix} \beta\{\psi\} \\ \{\psi\} \end{bmatrix} \tag{5}$$

where $[I]$ is an identity matrix. To estimate propagation loss, the computational window in transverse direction is terminated by the perfectly matched layer (PML) with thickness of 2 μm. An effective index n_e is defined by β/k_0 where $k_0 = 2\pi/\lambda$.

B. Characteristics of the SDDC

First, we investigate the standard SDDC ($r = 1$) so as to clear optimal dimensional parameters; the period length Λ, the amplitude of sinusoidal function A. Figure 2 shows real part of effective index of two TE-like super modes, $\mathrm{Re}(n_{TE,even})$ and $\mathrm{Re}(n_{TE,odd})$, as a function of sinusoidal amplitude. It can be seen that the effective indices of the super-modes increase as A does. The phase shift Φ per a period can be written by $\Phi = k_0 n_e L$, where n_e is an effective index of even- or odd mode in a straight DC, and $L = L(A, \Lambda)$ is path length of lightwave in a sinusoidal DC. If the light path is completely along with $f(z) = A\cos(2\pi z/\Lambda)$, L is written by

$$L(A,\Lambda) = \left\{ \frac{1}{\Lambda}\int_0^{\Lambda} \sqrt{1 + \left(\frac{2\pi A}{\Lambda}\right)^2 \sin^2\left(\frac{2\pi z}{\Lambda}\right)}\, dz \right\} \Lambda$$
$$\equiv \alpha(A,\Lambda)\Lambda. \tag{6}$$

The phase shift can be rewritten by $\Phi = k_0 n_e \alpha(A,\Lambda)\Lambda$, so the effective index of the super-modes in the sinusoidal DC can be represented by $n_e' = n_e\alpha(A,\Lambda) \geq n_e$. It seems that the effective indices of the super-modes increases as A does mainly because of this phase shift effects in the standard SDDC. Since the coupling length is $L_{c,TE} = \lambda/(2\Delta n_{TE})$ where $\Delta n_{TE} = |\mathrm{Re}(n_{TE,even}) - \mathrm{Re}(n_{TE,odd})|$, the power coupling to an adjacent waveguide can be prohibited by making Δn_{TE} be zero. According to the theoretical investigation in [16], the SDDC can make Δn_{TE} be zero, that is, the CDT condition can be satisfied by tuning A properly. In [16], it is revealed that the CDT condition can be written by

$$J_0\left(\frac{4\pi\kappa n_e A}{\Lambda}\right) = 0 \tag{7}$$

where J_0 is the zero-th order Bessel function of the first kind. κ is defined by

$$\kappa = k_0 \int_{-\infty}^{\infty} \psi_{even}^*(x')x'\psi_{odd}(x')dx' \tag{8}$$

where $x' = x - f(z)$, $\psi_{even/odd}$ is eigenmode field of even or odd mode in the straight DC. The first root of (7) is

$$A = 2.405\frac{\Lambda}{4\pi\kappa n_e}. \tag{9}$$

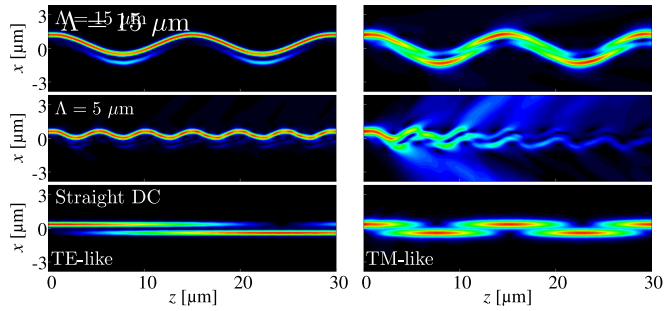

Fig. 3. Propagating electro-magnetic fields in the standard SDDCs satisfying $\Delta n_{\mathrm{TE}} = 0$, and the straight DC. The field is $|H_y|$ for TE-like wave, or $|E_y|$ for TM-like one.

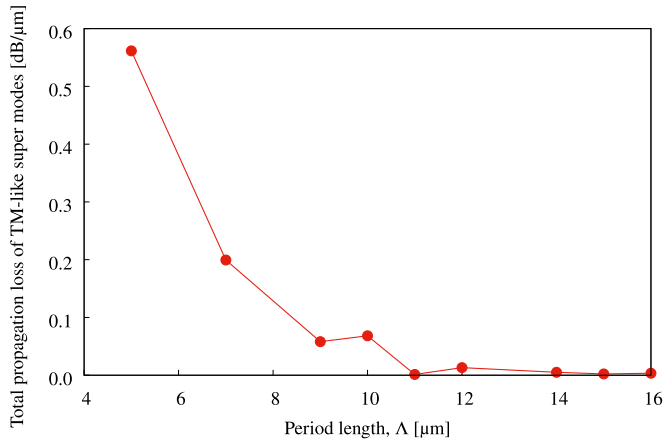

Fig. 4. Total propagation loss of TM-like super-modes in the standard SDDC ($r = 1$) as a function of period length Λ at $\lambda = 1.55$ μm.

As shown in Fig. 2, A to satisfy the CDT condition increases as Λ does, which is in accord with (9). However, (7) is extracted by the assumption of $\Lambda \ll L_{\mathrm{c}}$, and propagation loss is not taken into account. Thus, in practice, Λ has to be carefully chosen. Figure 3 shows the propagating electro-magnetic fields in the straight DC and the standard SDDC at $\Lambda = 5$ and 15 μm. In the SDDC shown in the figure, A is tuned so that $\Delta n_{\mathrm{TE}} = 0$. We can see that large Λ causes non-negligible power transfer of TE-like wave to an adjacent waveguide, but small Λ evokes large propagating loss of TM-like one though power coupling of TE-like one can be almost suppressed. This is because maximum curvature of waveguide $|\rho|_{\max}$ increases as Λ decreases when the CDT condition is satisfied:

$$|\rho|_{\max} = \max_z \left| \frac{f''(z)}{(1 + f'^2(z))^{1.5}} \right| = 2.405 \frac{\pi}{\kappa n_e \Lambda}. \qquad (10)$$

Thus, there is trade-off relation between crosstalk of TE-like wave and loss of TM-like one. Figure 4 shows total propagation loss per μm of TM-like super-modes as a function of Λ when $\Delta n_{\mathrm{TE}} = 0$. The total propagation loss is estimated by imaginary part of effective indices of TM-like super-modes: $-20k_0 \mathrm{Im}\{0.5(n_{\mathrm{TM,even}} + n_{\mathrm{TM,odd}})\}/\ln(10)$. We can see that shortest period length with low propagation loss is around $\Lambda = 11$ μm.

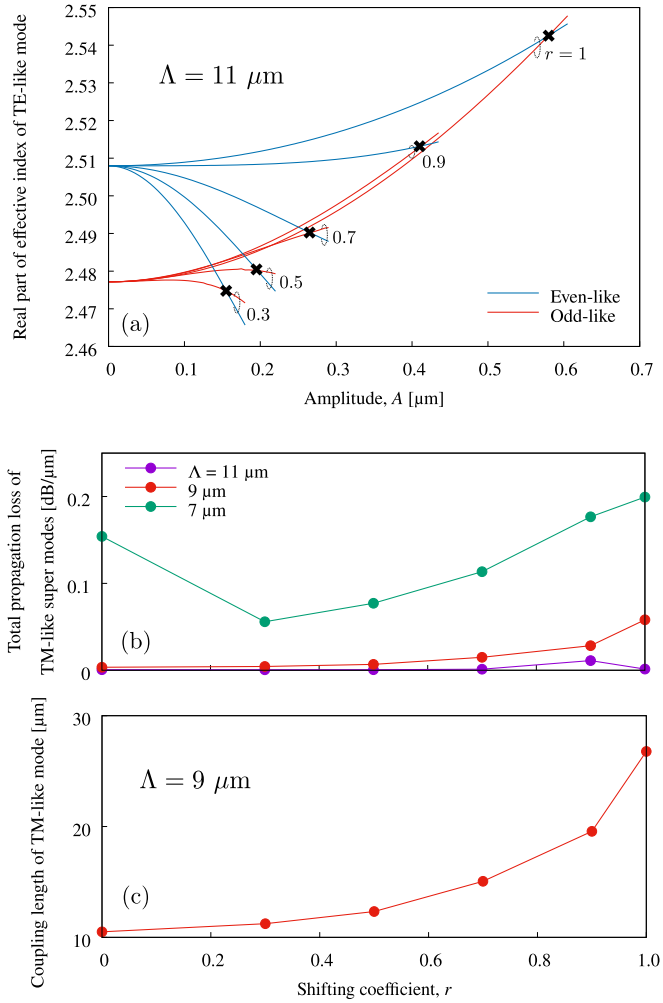

Fig. 5. The effect of the shifting coefficient r. (a) Effective indices of TE-like super-modes as a function of sinusoidal amplitude. Relation between r and (b) total propagation loss of TM-like super-modes and (c) the coupling length of TM-like wave ($\Lambda = 9$ μm) when $\Delta n_{\mathrm{TE}} = 0$. The characteristics shown in this figure is calculated at $\lambda = 1.55$ μm.

Next, we investigate effect of the shifting coefficient r, which shifts center position of the DC-gap. Figure 5(a) shows real part of effective indices of TE-like super-modes as a function of the sinusoidal amplitude at $\Lambda = 11$ μm. It can be seen that the cross point where $\Delta n_{\mathrm{TE}} = 0$ is shifted by r, and the amplitude satisfying the CDT condition can be small by tuning r. Therefore, the propagation loss of TM-like mode may be more suppressed even if Λ is short. Figure 5(b) shows the relation between r and the propagation loss when $\Delta n_{\mathrm{TE}} = 0$. Although the loss cannot be suppressed enough if Λ is too short, Λ can be shorter than the standard SDDC. Moreover, tuning r affects the coupling length of TM-like wave as shown in Fig. 5(c). We can see that the coupling length $L_{\mathrm{c,TM}}$ can be shorten by making r small. Thus, it is expected that tuning r results in enhancing the performance of the SDDC based PBS.

C. Analysis of the SDDC-Based PBS

In this sub-section, we compare whole characteristics of the standard SDDC and one tuning r. The SDDC-based PBS

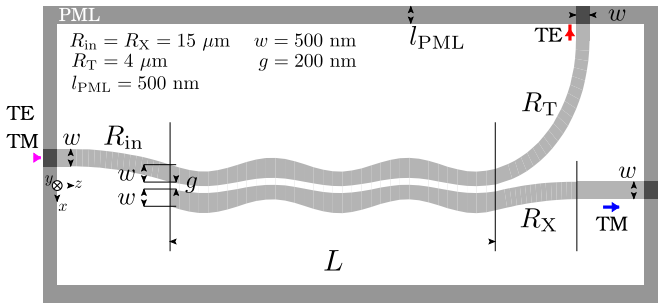

Fig. 6. A schematic of the SDDC-based PBS. L is length of SDDC section. R_{in}, R_T, and R_X are bending radius of input, through, and cross port waveguides, respectively.

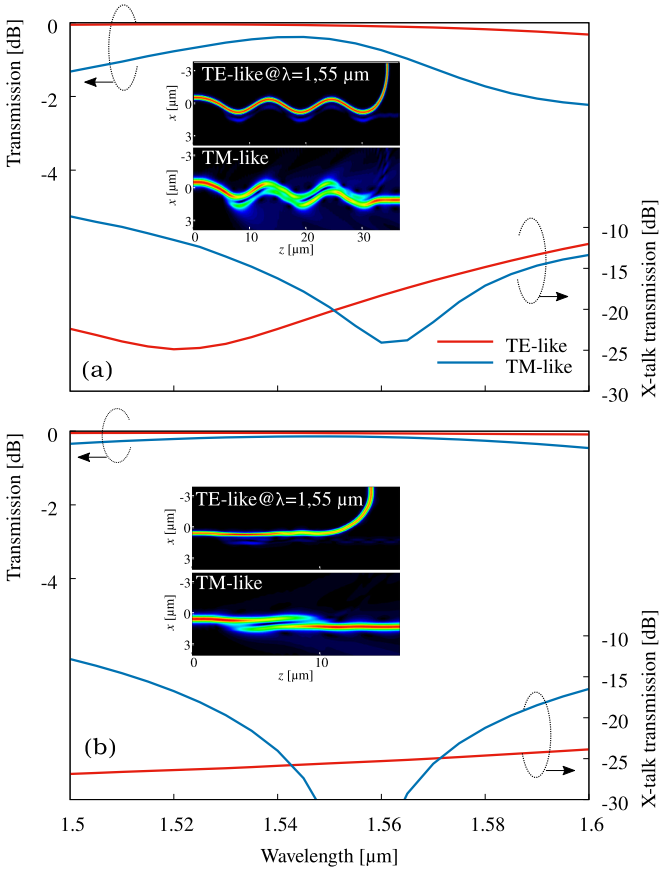

Fig. 7. Transmission spectra of (a) the standard SDDC-based PBS (SDDC-PBS1) and (b) the DC-gap-shifted one (SDDC-PBS2). Insets show electromagnetic fields in the SDDC-based PBS at $\lambda = 1.55\ \mu$m.

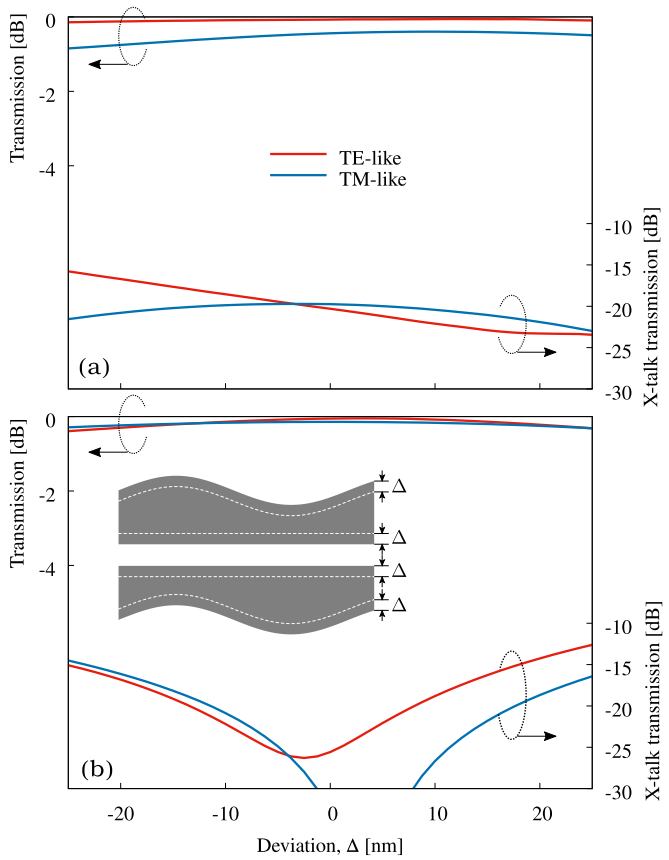

Fig. 8. Transmission as a function of deviation of core width and DC-gap, Δ in (a) SDDC-PBS1 and (b) SDDC-PBS2 at $\lambda = 1.55\ \mu$m. Core width and DC-gap are $w + 2\Delta$ and $g - 2\Delta$.

analyzed here is shown in Fig. 6. We investigate the transmission characteristics of a standard SDDC-based PBS (SDDC-PBS1: $\Lambda = 11\ \mu$m, $A = 0.58\ \mu$m, $r = 1$) and a DC-gap-shifted one (SDDC-PBS2: $\Lambda = 9\ \mu$m, $A = 0.135\ \mu$m, $r = 0$) using the 2DFEM with the EIM. The longitudinal length of the SDDC section L is taken to be $25.9\ \mu$m for the SDDC-PBS1, $7.8\ \mu$m for SDDC-PBS2, which are not exactly $L_{c,TM}$ and are tuned so that crosstalk transmission is minimized at $\lambda = 1.55\ \mu$m.

Figure 7 shows power transmission spectra of the two SDDC-PBSs. In the SDDC-PBS1, wavelength region where polarization extinction ratio (PER) is < -15 dB ranges from 1.54 to $1.575\ \mu$m, and insertion loss is < 1.5 dB in this range. As shown in 7(b), flat crosstalk transmission is obtained for TE-like wave in the SDDC-PBS2, and < -15 dB PER ranges from 1.515 to $1.6\ \mu$m, and insertion loss is < 0.46 dB. Furthermore, the SDDC-PBS2 achieves < -20 dB PER and insertion loss of < 0.26 dB from 1.535 to $1.58\ \mu$m. Figure 8 shows effects of waveguide sidewall deviation Δ on transmission characteristics at $\lambda = 1.55\ \mu$m. Positive Δ indicates under-etching, and negative one does over-etching. The SDDC-PBS1 maintains PER of < -15 dB and insertion loss of < 0.84 dB in the shown range, and < -20 dB PER region ranges from $\Delta = 10$ to 25 nm. In the SDDC-PBS2, < -15 dB PER region ranges from $\Delta = -22.5$ to 17.5 nm, and insertion loss is < 0.34 dB in the range. In region from $\Delta = -10$ to 7.5 nm, < -20 dB PER and insertion loss of < 0.166 dB is accomplished.

One advantage of the DC-based PBS is the simplicity of device configuration. The PBS using the simple straight DC is reported in [8], and it is experimentally demonstrated that this PBS has ~ -15 dB PER at wavelength range of 1.5–1.6 μm with < 0.5 dB excess loss. Unwanted power coupling causes inherently in the PBS based on the simple DC, so in the report two PBSs are cascaded to improve PER, which results in larger footprint in longitudinal direction ($16\ \mu$m $\times 2$). In order to suppress the coupling of TE-like wave to an adjacent waveguide, slot waveguide is utilized in [14], but slot-to-strip convert section

is necessary. Use of point-symmetric-DC [11] is attractive in terms of broadband operation, and < -20 dB PER at range of 1.477–1.602 μm is experimentally demonstrated. However, much longer device length (97.4 μm) is required because it consists of two 3 dB couplers and phase shift section like the MZI. Recently, to make DC coupling section shorter, the PBS based on bent DC is reported [9], [10], [13], [14]. Especially, in [14], ultra-compact footprint (4.9 μm) is achieved, and experimental results show this PBS has < -14 dB crosstalk and ~ 0.55 dB insertion loss at range of 1.509–1.59 μm. This PBS is also based on an adiabatically tapering (AT) DC, which can improve fabrication tolerance. The gap-shifted SDDC-PBS may posses the advantages of PBS based on slot waveguide, bent one, and AT-DC. It can suppress the unwanted coupling owing to the CDT effects as shown in Fig. 7(b), and fabrication tolerance may be enhanced because the waveguide width is adiabatically changed in the coupling section. Moreover, shifting the DC-gap can make the device length shorter. Although some complexity has to be added comparing with the simple DC, the gap-shifted SDDC has potential to improve the PER of TE-like wave, fabrication tolerance, and miniaturize footprint.

III. Conclusion

In this paper, we numerically investigate characteristics of SDDC-based PBS, and the effects of DC-gap shift r. We discuss trade-off relation between crosstalk of TE-like wave and loss of TM-like one, and show one way to determine optimal sinusoidal period length Λ in the standard SDDC and the gap-shifted SDDC. The numerical results show potential to enhance the figure of merit of SDDC-based PBS and to achieve smaller-footprint by shifting DC-gap position.

Appendix

In the waveguide shown in Fig. 1, the govern equation is

$$\frac{1}{s_x}\frac{\partial}{\partial x}\left(\frac{p}{s_x}\frac{\partial \phi}{\partial x}\right)+\frac{\partial}{\partial z}\left(p\frac{\partial \phi}{\partial z}\right)+k_0^2 q\phi = 0 \tag{11}$$

with

$$p=\begin{Bmatrix}1\\ \varepsilon_r^{-1}\end{Bmatrix},\quad q=\begin{Bmatrix}\varepsilon_r\\ 1\end{Bmatrix},\quad \phi=\begin{Bmatrix}E_y\\ H_y\end{Bmatrix}$$

where ε_r is relative permittivity. s_x is a PML stretching coefficient that we define as

$$s_x=\begin{cases}1-\mathrm{j}\left(\frac{x_\mathrm{L}-x}{l_{\mathrm{L,PML}}}\right)^2\tan\delta & [x<x_\mathrm{L}]\\ 1 & [x_\mathrm{L}\le x\le x_\mathrm{R}]\\ 1-\mathrm{j}\left(\frac{x-x_\mathrm{R}}{l_{\mathrm{R,PML}}}\right)^2\tan\delta & [x_\mathrm{R}<x]\end{cases} \tag{12}$$

where $x_{\mathrm{L/R}}$ is position of surface between physical window and the PML, $l_{\mathrm{L/R,PML}}$ is thickness of the PML, and $\tan\delta$ is a loss tangent. In this paper, the computational domain is descritized by triangular elements with 2nd order. The electro-magnetic field in a local element is expanded by

$$\begin{aligned}\phi(x,z)&=\psi(x,z)\exp(-\mathrm{j}\beta z)\\ &=\exp(-\mathrm{j}\beta z)\left\{N(x,z)\right\}^T\left\{\tilde{\psi}\right\}\equiv\left\{\tilde{N}\right\}^T\left\{\tilde{\psi}\right\}\end{aligned} \tag{13}$$

where $\{N\}$ is a shape function, and $\{\tilde{\psi}\}$ is a vector whose component is ψ at element node position. Applying the Galerkin method to (11), the following system of equations can be obtained

$$[\tilde{P}]\{\tilde{\psi}\}=\left([\tilde{K}]+\beta[\tilde{D}]-\beta^2[\tilde{M}]\right)\{\tilde{\psi}\}=\{\tilde{u}\} \tag{14}$$

with

$$\begin{aligned}[\tilde{K}]=\sum_e\iint_e\Big[&-\frac{p}{s_x}\{N\}_x\{N\}_x^T\\ &-ps_x\{N\}_z\{N\}_z^T+k_0^2qs_x\{N\}\{N\}^T\Big]dxdz\end{aligned} \tag{15}$$

$$[\tilde{D}]=\sum_e\iint_e \mathrm{j}ps_x\left(\{N\}_z\{N\}^T-\{N\}\{N\}_z^T\right)dxdz \tag{16}$$

$$[\tilde{M}]=\sum_e\iint_e ps_x\{N\}\{N\}^T dxdz \tag{17}$$

$$\begin{aligned}\{\tilde{u}\}=&-\sum_e{}'\int_{\Gamma_{\mathrm{L,e}}}\{\tilde{N}\}^* ps_x\frac{\partial\phi}{\partial z}dx\\ &+\sum_e{}'\int_{\Gamma_{\mathrm{R,e}}}\{\tilde{N}\}^* ps_x\frac{\partial\phi}{\partial z}dx\end{aligned} \tag{18}$$

where $\{N\}_\alpha(\alpha=x,z)$ denotes $\partial\{N\}/\partial\alpha$. This can be represented by

$$\begin{bmatrix}[\tilde{P}]_{00} & [\tilde{P}]_{0\mathrm{L}} & [\tilde{P}]_{0\mathrm{R}}\\ [\tilde{P}]_{\mathrm{L}0} & [\tilde{P}]_{\mathrm{LL}} & [\tilde{P}]_{\mathrm{LR}}\\ [\tilde{P}]_{\mathrm{R}0} & [\tilde{P}]_{\mathrm{RL}} & [\tilde{P}]_{\mathrm{RR}}\end{bmatrix}\begin{Bmatrix}\{\tilde{\psi}\}_0\\ \{\tilde{\psi}\}_\mathrm{L}\\ \{\tilde{\psi}\}_\mathrm{R}\end{Bmatrix}=\begin{Bmatrix}\{0\}\\ -\{\tilde{u}\}_\mathrm{L}\\ \{\tilde{u}\}_\mathrm{R}\end{Bmatrix}. \tag{19}$$

Since Γ_L and Γ_R are periodic boundaries, $\{\tilde{\psi}\}_\mathrm{L}=\{\tilde{\psi}\}_\mathrm{R}=\{\psi\}_\Gamma$ and $\{\tilde{u}\}_\mathrm{L}=\{\tilde{u}\}_\mathrm{R}$ holds, thus equations in (19) can be reduced.

$$\begin{bmatrix}[\tilde{P}]_{00} & [P]_{0\Gamma}\\ [P]_{\Gamma 0} & [P]_{\Gamma\Gamma}\end{bmatrix}\begin{Bmatrix}\{\tilde{\psi}\}_0\\ \{\psi\}_\Gamma\end{Bmatrix}=\{0\}. \tag{20}$$

This is the quadratic eigenvalue equation (1) and the system matrices $[K]$, $[D]$, $[M]$, and the solution vector $\{\psi\}$ are represented by

$$[K]=\begin{bmatrix}[\tilde{K}]_{00} & [K]_{0\Gamma}\\ [K]_{\Gamma 0} & [K]_{\Gamma\Gamma}\end{bmatrix} \tag{21}$$

$$[D]=\begin{bmatrix}[\tilde{D}]_{00} & [D]_{0\Gamma}\\ [D]_{\Gamma 0} & [D]_{\Gamma\Gamma}\end{bmatrix} \tag{22}$$

$$[M]=\begin{bmatrix}[\tilde{M}]_{00} & [M]_{0\Gamma}\\ [M]_{\Gamma 0} & [M]_{\Gamma\Gamma}\end{bmatrix} \tag{23}$$

$$\{\psi\}=\begin{Bmatrix}\{\tilde{\psi}\}_0\\ \{\psi\}_\Gamma\end{Bmatrix} \tag{24}$$

$$[K]_{0\Gamma}=[\tilde{K}]_{0\mathrm{L}}+[\tilde{K}]_{0\mathrm{R}} \tag{25}$$

$$[K]_{\Gamma 0}=[\tilde{K}]_{\mathrm{L}0}+[\tilde{K}]_{\mathrm{R}0} \tag{26}$$

$$[K]_{\Gamma\Gamma}=[\tilde{K}]_{\mathrm{LL}}+[\tilde{K}]_{\mathrm{LR}}+[\tilde{K}]_{\mathrm{RL}}+[\tilde{K}]_{\mathrm{RR}} \tag{27}$$

$$[D]_{0\Gamma} = [\tilde{D}]_{0\mathrm{L}} + [\tilde{D}]_{0\mathrm{R}} \tag{28}$$

$$[D]_{\Gamma 0} = [\tilde{D}]_{\mathrm{L}0} + [\tilde{D}]_{\mathrm{R}0} \tag{29}$$

$$[D]_{\Gamma\Gamma} = [\tilde{D}]_{\mathrm{LL}} + [\tilde{D}]_{\mathrm{LR}} + [\tilde{D}]_{\mathrm{RL}} + [\tilde{D}]_{\mathrm{RR}} \tag{30}$$

$$[M]_{0\Gamma} = [\tilde{M}]_{0\mathrm{L}} + [\tilde{M}]_{0\mathrm{R}} \tag{31}$$

$$[M]_{\Gamma 0} = [\tilde{M}]_{\mathrm{L}0} + [\tilde{M}]_{\mathrm{R}0} \tag{32}$$

$$[M]_{\Gamma\Gamma} = [\tilde{M}]_{\mathrm{LL}} + [\tilde{M}]_{\mathrm{LR}} + [\tilde{M}]_{\mathrm{RL}} + [\tilde{M}]_{\mathrm{RR}}. \tag{33}$$

REFERENCES

[1] L. B. Soldano, A. I. Vreede, M. K. Smit, B. H. Verbeek, E. G. Metaal, and F. H. Green, "Mach-Zehnder interferometer polarization splitter in InGaAsP/InP," *IEEE Photon. Technol. Lett*., vol. 6, no. 3, pp. 402–405, Mar. 1994.

[2] T. K. Liang and H. K. Tsang, "Integrated polarization beam splitter in high index contrast silicon-on-insulator waveguides," *IEEE Photon. Technol. Lett*., vol. 17, no. 2, pp. 393–395, Feb. 2005.

[3] D. Dai, Z. Wang, and J. E. Bowers, "Considerations for the design of asymmetrical Mach-Zehnder interferometers used as polarization beam splitters on a submicrometer silicon-on-insulator platform," *J. Lightw. Technol*., vol. 29, no. 12, pp. 1808–1817, Jun. 2011.

[4] J. M. Hong *et al.*, "Design and fabrication of a significantly shortened multimode interference coupler for polarization splitter application," *IEEE Photon. Technol. Lett*., vol. 15, no. 1, pp. 72–74, Jan. 2003.

[5] A. Katigbak, J. F. Strother Jr., and J. Lin, "Compact silicon slot waveguide polarization splitter," *Opt. Eng*., vol. 8, no. 8, pp. 1–3, Aug. 2009.

[6] M. Yin, W. Yang, Y. Li, X. Wang, and H. Li, "CMOS-compatible and fabrication-tolerant MMI-based polarization beam splitter," *Opt. Commun*., vol. 335, pp. 48–52, Jan. 2015.

[7] I. Kiyat, A. Aydinli, and N. Dagli, "A compact silicon-on-insulator polarization splitter," *IEEE Photon. Technol. Lett*., vol. 17, no. 1, pp. 100–102, Jan. 2005.

[8] H. Fukuda, K. Yamada, T. Tsuchizawa, T. Watanabe, H. Shinojima, and S. Itabashi, "Ultrasmall polarization splitter based on silicon wire waveguides," *Opt. Exp.*, vol. 14, no. 25, pp. 12401–12408, Dec. 2006.

[9] D. Dai and J. E. Bowers, "Novel ultra-short and ultra-broadband polarization beam splitter based on a bent directional coupler," *Opt. Exp.*, vol. 19, no. 19, pp. 18614–18620, Sep. 2011.

[10] J. Wang, D. Liang, Y. Tang, D. Dai, and J. E. Bowers, "Realization of an ultra-short silicon polarization beam splitter with an asymmetrical bent directional coupler," *Opt. Lett*., vol. 38, no. 1, pp. 4–6, Jan. 2013.

[11] Z. Lu, Y. Wang, F. Zhang, N. A. F. Jaeger, and L. Chrostowski, "Wideband silicon photonic polarization beamsplitter based on pointsymmetric cascaded broadband couplers," *Opt. Exp.*, no. 23, vol. 23, pp. 29413–29422, Nov. 2015.

[12] J. Feng, R. Akimoto, and H. Zeng, "Asymmetric silicon slot-waveguide assisted polarizing beam splitter," *IEEE Photon. Technol. Lett.*, vol. 28, no. 12, pp. 1294–1297, Jun. 2016.

[13] H. Wu, Y. Tan, and D. Dai, "Ultra-broadband high-performance polarizing beam splitter on silicon," *Opt. Exp.*, vol. 25, no. 6, pp. 6069–6075, Mar. 2017.

[14] J. Zhu *et al.*, "Ultra-compact mode (de)multiplexer and polarization beam splitter based on tapered bent asymmetric directional couplers," *IEEE Photon. J*., vol. 14, no. 1, Feb. 2022, Art no. 2206106.

[15] F. Zhang, H. Yun, Y. Wang, Z. Lu, L. Chrostowski, and N. A. F. Jaeger, "Compact broadband polarization beam splitter using a symmetric directional coupler with sinusoidal bends," *Opt. Lett*., vol. 42, no. 2, pp. 235–238, Jan. 2017.

[16] S. Longhi, "Coherent destruction of tunneling in waveguide directional couplers," *Phys. Rev. A*, vol. 71, no. 6, pp. 1–4, Jun. 2005.

[17] Y. Tsuji and M. Koshiba, "Finite element method using port truncation by perfectly matched layer boundary conditions for optical waveguide discontinuity problems," *J. Lightw. Technol*., vol. 20, no. 3, pp. 463–468, Mar. 2002.

[18] K. Okamoto, *Fundamentals of Optical Waveguides*, 2nd ed., Burlington, VT, USA: Academic Press, 2006.

[19] C. Z. Tan, "Determination of refractive index of silica glass for infrared wavelengths by IR spectroscopy," *J. Non-Cryst. Solids*, vol. 223, no. 1, pp. 158–163, Jan. 1998.

[20] H. H. Li, "Refractive index of silicon and germanium and its wavelength and temperature derivatives," *J. Phys. Chem. Ref. Data*, vol. 9, no. 3, pp. 561–658, 1980.